Supporting Information

Wang et al. 10.1073/pnas.1214626110

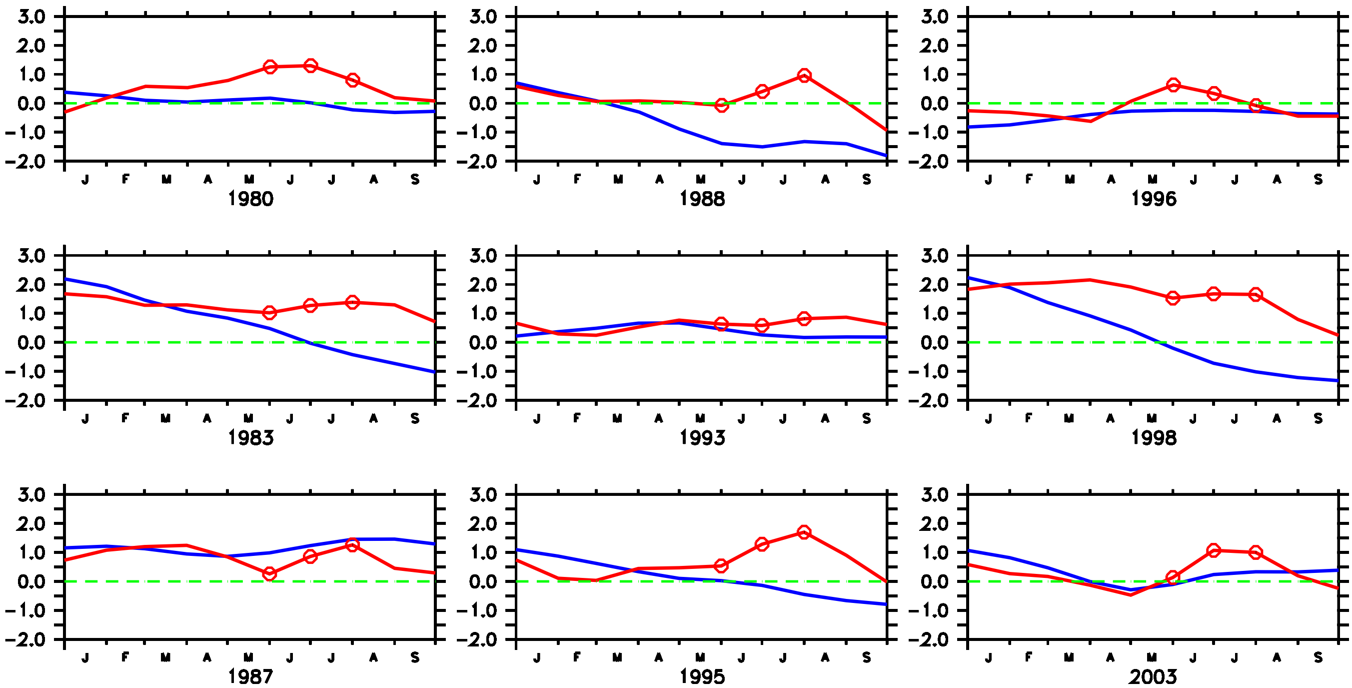

Fig. S1. Relationship between strong western Pacific Subtropical High (WPSH) and El Niño decay. Plotted are 3-mo running mean WPSH index (red) and Niño3.4 sea surface temperature anomaly (SSTA) (°C) (5°S–5°N, 170°W–120°W, blue) from January to October for the nine strong WPSH years. June-July-August (JJA) season is indicated by the circles. Note that only five cases (1983, 1988, 1995, 1998, and 2003) occurred during El Niño decay summers.

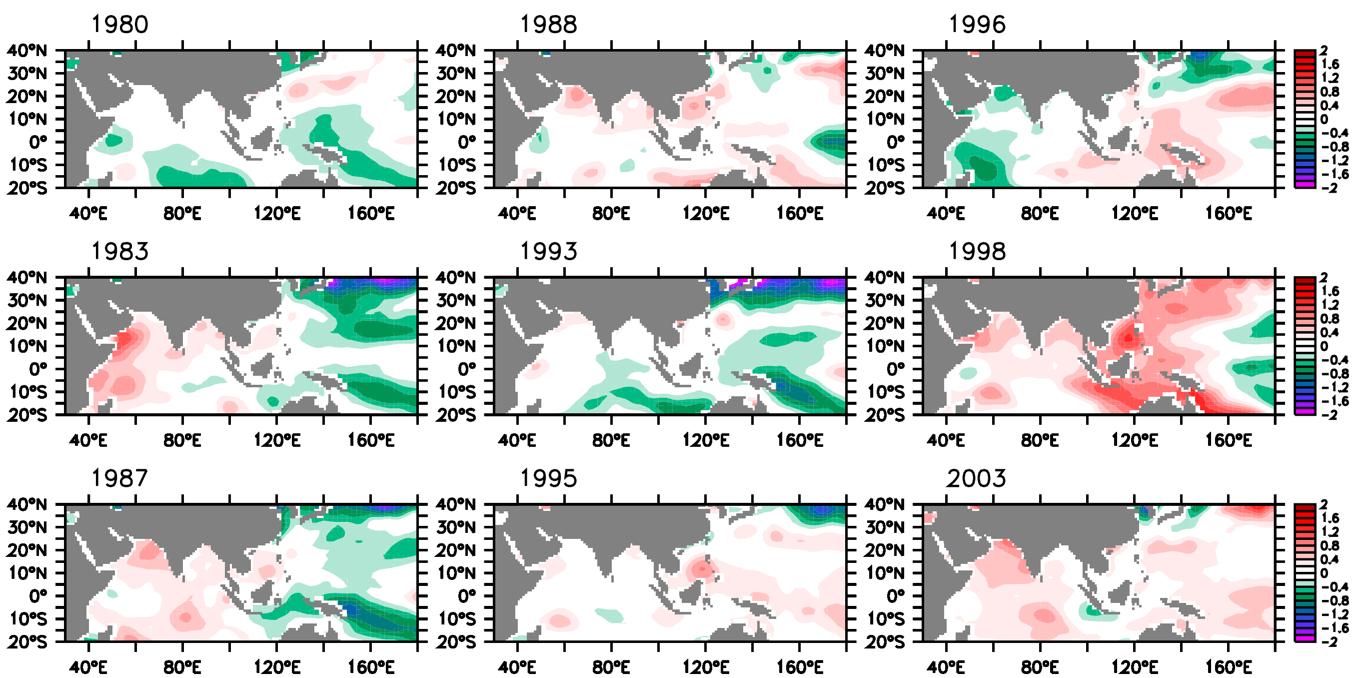

Fig. S2. Relationship between the strong WPSH and Indian Ocean (IO) warming. Summer (JJA) mean SSTA for the nine strong WPSH years. Note that four cases are not accompanied by IO warming (1980, 1993, 1995, and 1996).

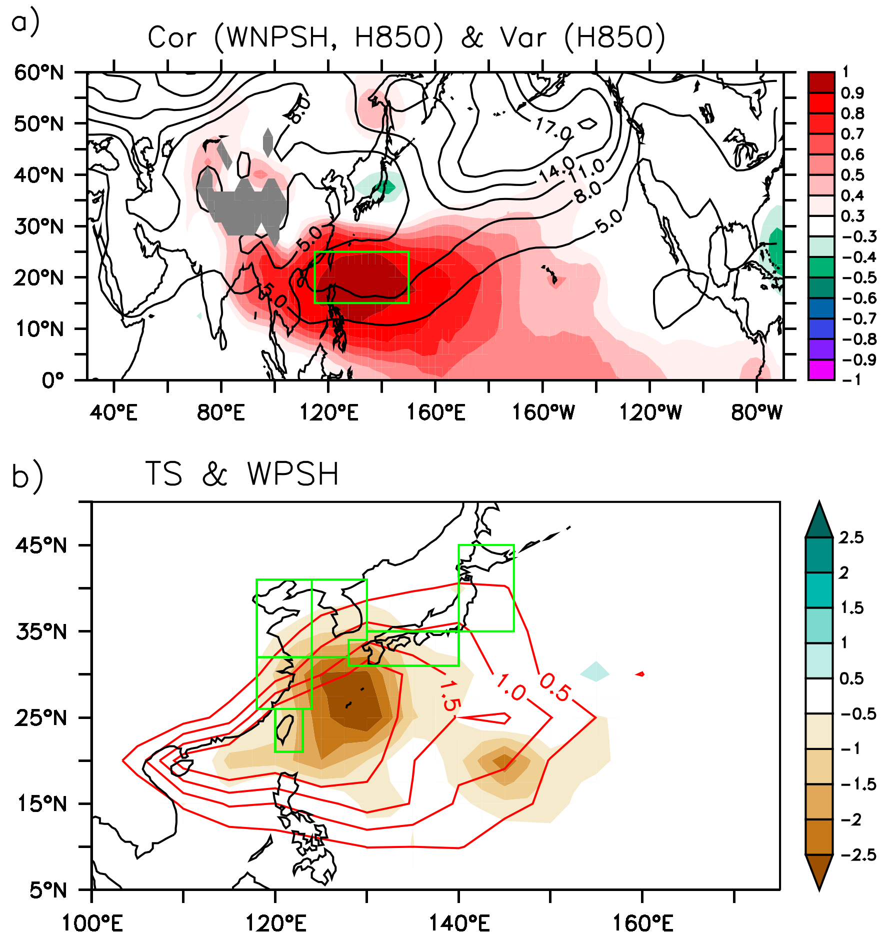

Fig. S3. (*A*) Definition of the WPSH Index. The contours (units: m) show interannual SD of JJA H850. The green box shows the region where the WPSH index is defined and coincides with the region of maximum interannual variation in the subtropical Pacific. (*B*) Relationships between the WPSH index and tropical storm (TS) activities. The composite difference maps between the four strongest and four weakest WPSH years during 1979–2009 in TS days (shading) along with the climatological JJA mean TS days (contours). The units for TS days are days per year. The six green boxes show the East Asian coastal regions. The total TS numbers impacting these six coastal regions have a significant correlation with the WPSH index ($r = -0.76$).

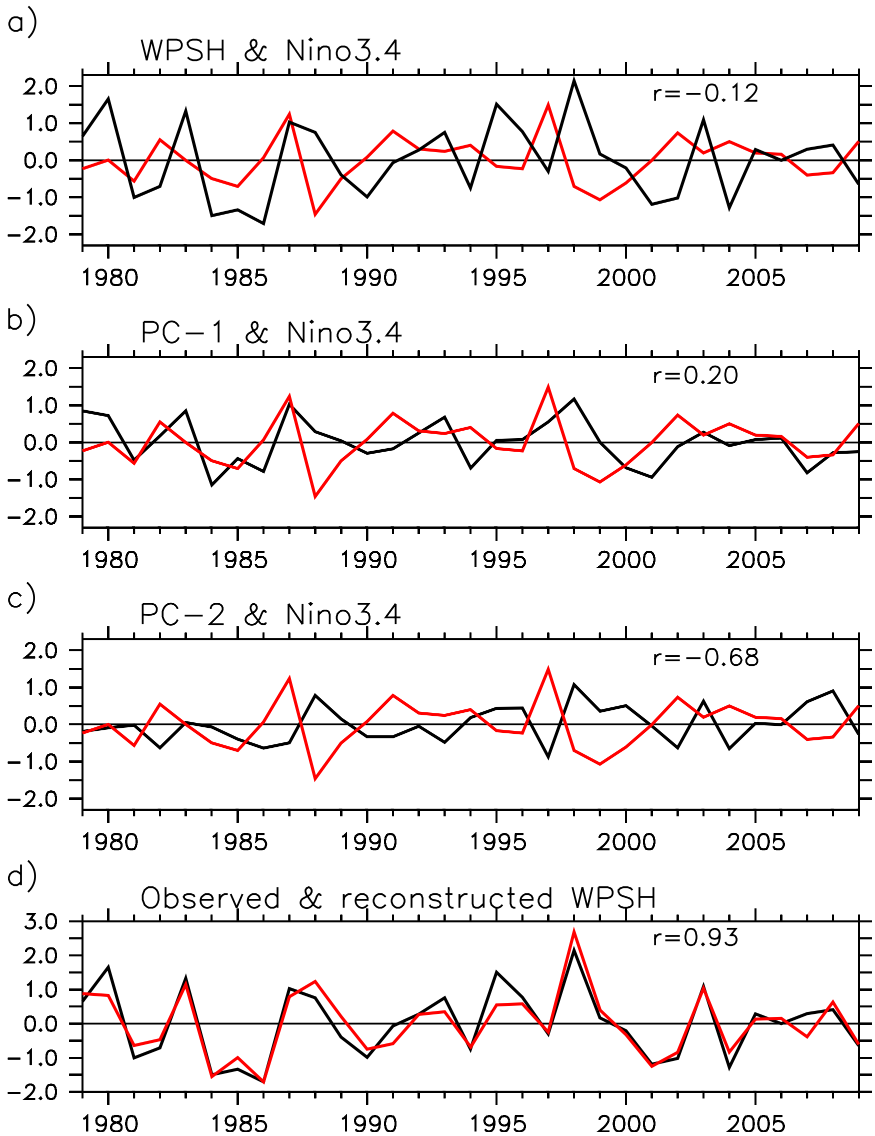

Fig. S4. Relationships among the Niño3.4 index, the WPSH index and the two principal components (PCs). The black in *A–C* denotes the WPSH index, PC-1, and PC-2 time series, respectively. The red represents the Niño3.4 index. Note that the WPSH and PC-1 are not significantly correlated with Niño3.4 index ($r = -0.12$ and 0.20, respectively), whereas the PC-2 is significantly correlated with the Niño3.4 index ($r = -0.68$). In fact, the majority of the strong positive years in PC-2 is in accord with developing or persisting La Niña events (1988, 1995, 1996, 1998, 1999, 2000, 2007, and 2008), whereas the strong negative years in PC-2 concur with El Niño development (1982, 1986, 1997, 2002, and 2004). (*D*) Reconstruction of the WPSH index using two PCs based on the multivariate regression. The observed WPSH index (black) and the reconstructed (red) index based on PC-1 and PC-2 (1.289×PC-1 + 1.099×PC-2). Their correlation coefficient is 0.93.

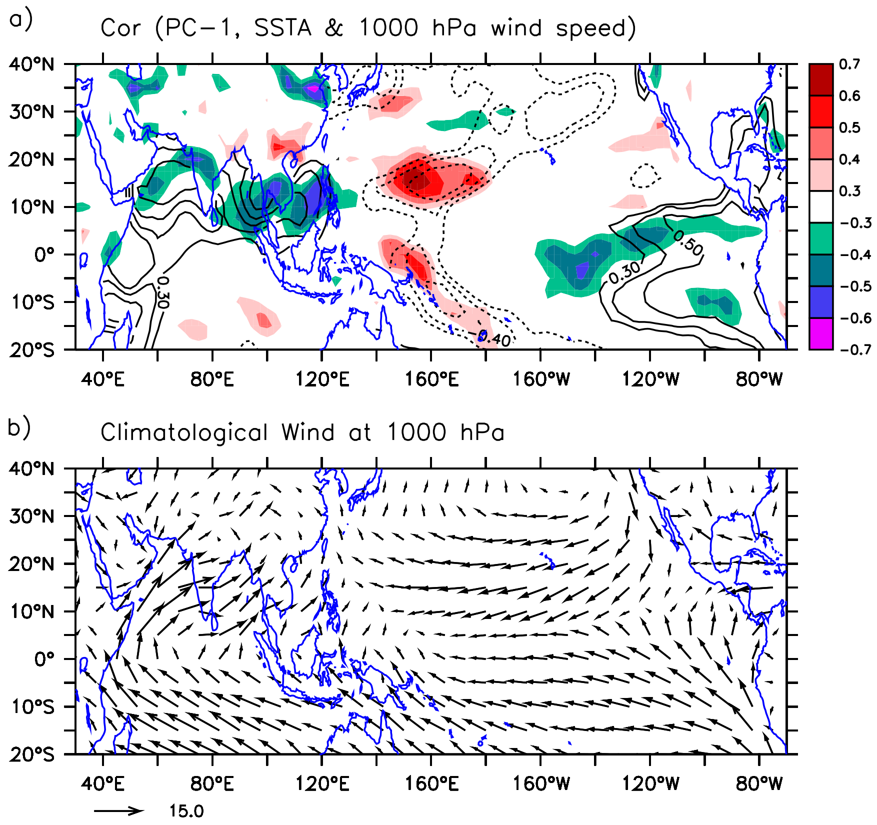

Fig. S5. Evidence for WPSH affecting sea surface temperature (SST). (*A*) Shown are the simultaneous correlation map of the 1,000 hPa wind speed anomaly (shading) and the SSTA (contours) with reference to the PC-1 of H850 anomaly. Note that when WPSH is strong, the total surface wind speed increases while the SST decreases to the southeast of the WPSH anomaly; conversely, the total wind speed decreases while SST increases to the southwest of the WPSH anomaly over the northern IO. This figure provides an evidence for the atmospheric influence on SST. (*B*) Climatological 1,000 hPa wind in boreal summer (JJA) from observation.

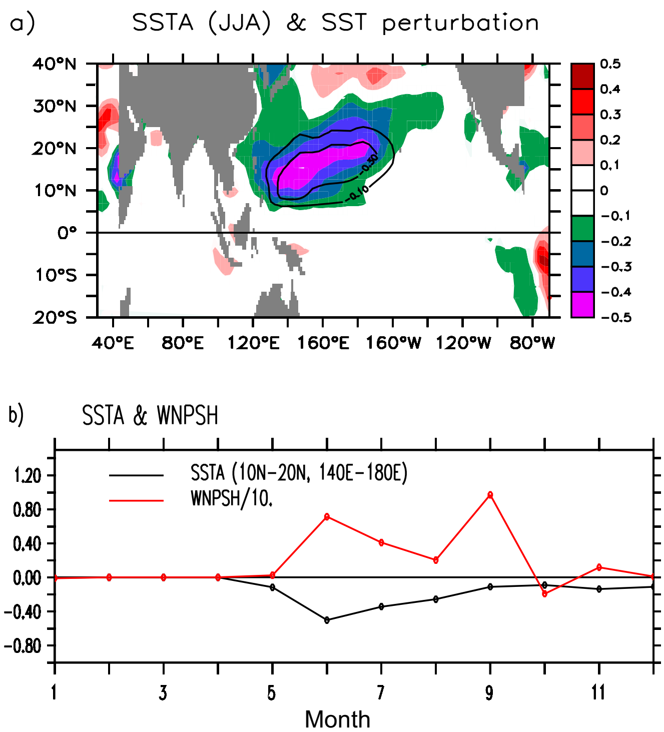

Fig. S6. Coupled model experiments showing how the atmosphere–ocean interaction maintains the anomalous WPSH. (*A*) An initial SST tendency perturbation (contours in °C per pentad) was imposed to the coupled model POEM from May 21 to May 31. After May 31, the model becomes freely coupled. Shading denotes the JJA SSTA relative to the control run. (*B*) Daily mean WNP (10°N–20°N, 140°E–180°E) SSTA (black) and 21-d running mean WPSH index (red) relative to the control run. The failure to reproduce the IO warming in the coupled model is likely due to the mean precipitation bias in the WNP that tends to anchor the anomalous WPSH northeastward compared with observations.

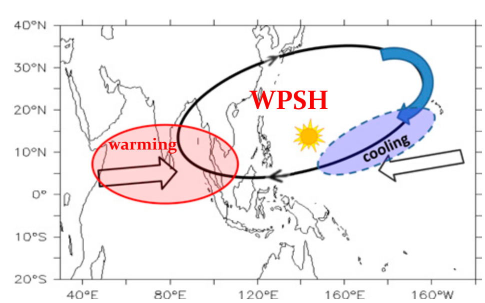

Fig. S7. Schematic diagram showing the atmosphere-ocean thermodynamic feedback between the WPSH (solid circle with arrows) and the underlying SST dipole (warming over the northern IO and cooling over the WNP). The sum of the anomalous winds and the mean winds (denoted by the double empty arrows) results in enhanced (reduced) total wind speed that cools (warms) the WNP (northern IO). However, the cooling in the WNP suppresses convection (denoted by the sun sign) that, in turn, generates descent atmospheric Rossby waves strengthening the WPSH. The warming in the northern IO also favors an enhanced WPSH by generating an anticyclonic vorticity associated with an atmospheric Kelvin wave response to the east of the northern IO warming.

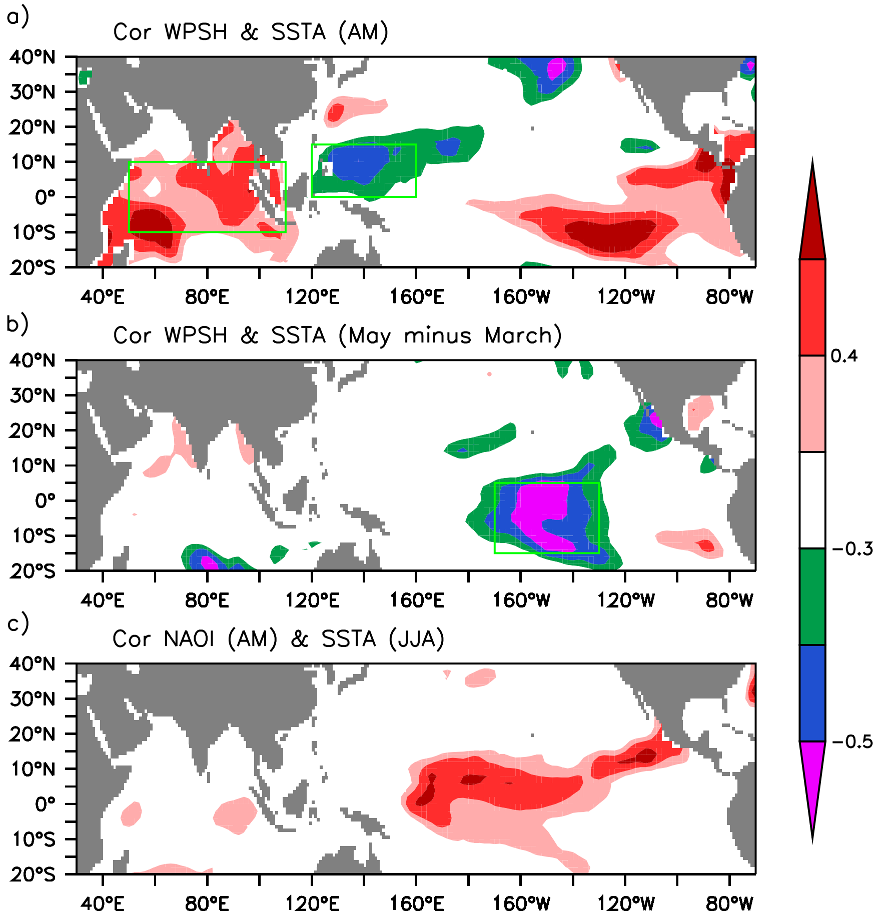

Fig. S8. Selection of predictors for the WPSH index based on the dynamics of the two empirical orthogonal function (EOF) modes and the correlation maps among the WPSH (JJA) index and the April-May mean SSTA (*A*), the WPSH (JJA) index and the May-minus-March SSTA (*B*), and the North Atlantic Oscillation (NAO) (April–May) index and boreal summer (JJA) SSTA (*C*). Only values with significance level above 90% are shown. The boxes in *A* and *B* indicate the areas where area-averaged SSTA is selected for construction of the corresponding predictors.

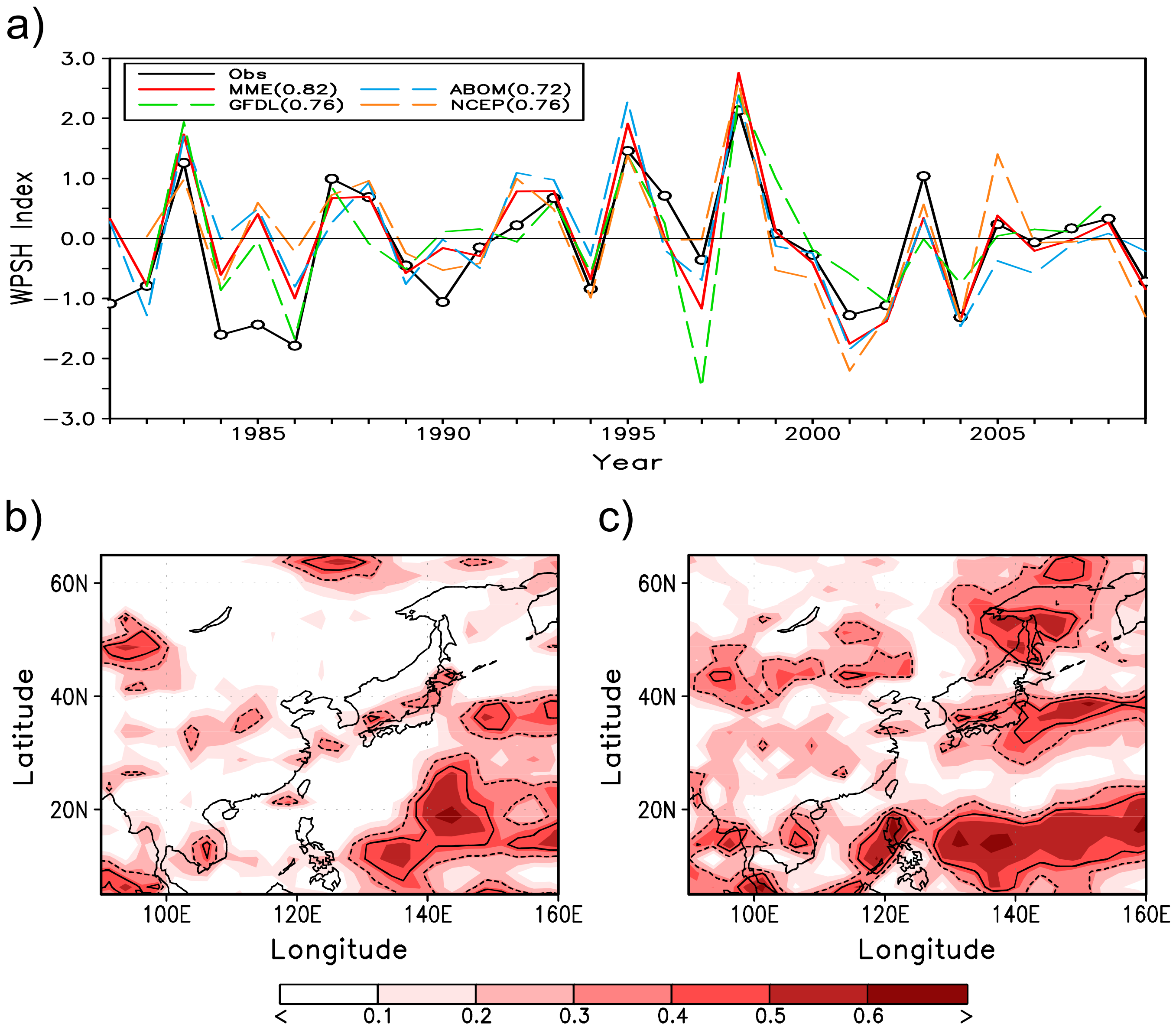

Fig. S9. (*A*) The time series of the observed WPSH index (black) from 1981 to 2009 and the multimodel ensemble (MME) hindcast result (red) using the June first initial condition. Results from three individual models [National Center for Environmental Prediction (NCEP), Geophysical Fluid Dynamics Laboratory (GFDL), Australian Bureau of Meteorology (ABOM)] are also shown by long-dashed lines. The correlation coefficient between the observed WPSH index and the predicted counterpart by MME, NCEP, GFDL, and ABOM are 0.82, 0.76, 0.76, and 0.72, respectively. The hindcast experiments data were provided by NCEP (1), GFDL (2), and ABOM (3) through APEC Climate Center (APCC)/climate prediction and application to society (CliPAS) project (4). (*B*) The temporal correlation skill (TCS) of the three dynamical model (4) ensemble reforecast of the JJA mean precipitation for the period 1981–2009 with June 1 initial condition. (*C*) Same as in *B*, but made by the empirical model; the precipitation is predicted by the product of the predicted WPSH index and the regressed precipitation onto the observed WPSH index. Dashed (solid) contour indicates significant TCS at 95% (99%) confident level.

1. Saha S, et al. (2006) The NCEP Climate Forecast System. *J Clim* 19:3483–3517.
2. Delworth TL, et al. (2006) GFDL's CM2 global coupled climate models. Part I: Formulation and simulation characteristics. *J Clim* 19:643–674.
3. Zhong A, Hendon HH, Alves O (2005) Indian Ocean variability and its association with ENSO in a global coupled model. *J Clim* 18:3634–3649.
4. Lee J-Y, et al. (2011) How predictable is the Northern Hemisphere summer upper-tropospheric circulation? *Clim Dyn* 37:1189–1203.

Table S1. Comparison of the WPSH indices

	WPSH index	EASM strength	WNP TS days	TS affecting EA coast
WPSH index	1	**–0.92**	**–0.81**	**–0.76**
Area index	0.67	−0.55	−0.40	−0.36
Intensity index	0.69	−0.56	−0.46	−0.39
North Edge index	−0.08	0.27	0.20	0.20
Mean Ridge index	−0.38	0.55	0.47	0.47
Westward Extension index	−0.76	0.64	0.56	0.48
WPSH index in Sui et al. (1) and Wu and Zhou (2)	0.86	−0.80	−0.81	−0.71

Shown in the table are correlation coefficients of seven WPSH indices with East Asian (EA) summer monsoon (EASM) strength, TS days in the subtropical WNP, and the total TS number impacting EA Cost (see Fig. S3*B* for the impacting region). The highest correlation coefficients are in bold. The WPSH index is defined in the present study. The middle five indices are used by the National Climate Center, China (http://ncc.cma.gov.cn/cn).

1. Sui C-H, Chung P-H, Li T (2007) Interannual and interdecadal variability of the summertime western North Pacific subtropical high. *Geophys Res Lett* 34:L11701, 10.1029/2006GL029204.
2. Wu B, Zhou T (2008) Oceanic origin of the interannual and interdecadal variability of the summertime western Pacific subtropical high. *Geophys Res Lett* 35:L13701.